Simulated variability of the circulation in the North Atlantic from 1953 to 2003

Julie Deshayes, Claude Frankignoul

Simulated Variability of the Circulation in the North Atlantic from 1953 to 2003

JULIE DESHAYES AND CLAUDE FRANKIGNOUL

LOCEAN, IPSL, Universite Pierre et Marie Curie, Paris, France

(Manuscript received 5 February 2007, in final form 3 March 2008)

ABSTRACT

The variability of the circulation in the North Atlantic and its link with atmospheric variability are investigated in a realistic hindcast simulation from 1953 to 2003. The interannual-to-decadal variability of the subpolar gyre circulation and the Meridional Overturning Circulation (MOC) is mostly influenced by the North Atlantic Oscillation (NAO). Both circulations intensified from the early 1970s to the mid-1990s and then decreased. The monthly variability of both circulations reflects the fast barotropic adjustment to NAO-related Ekman pumping anomalies, while the interannual-to-decadal variability is due to the baroclinic adjustment to Ekman pumping, buoyancy forcing, and dense water formation, consistent with previous studies.

An original characteristic of the oceanic response to NAO is presented that relates to the spatial patterns of buoyancy and wind forcing over the North Atlantic. Anomalous Ekman pumping associated with a positive NAO phase first induces a decrease of the southern subpolar gyre strength and an intensification of the northern subpolar gyre. The latter is reinforced by buoyancy loss and dense water formation in the Irminger Sea, where the cyclonic circulation increases 1–2 yr after the positive NAO phase. Increased buoyancy loss also occurs in the Labrador Sea, but because of the early decrease of the southern subpolar gyre strength, the intensification of the cyclonic circulation is delayed. Hence the subpolar gyre and the MOC start increasing in the Irminger Sea, while in the Labrador Sea the circulation at depth leads its surface counterpart. In this simulation where the transport of dense water through the North Atlantic sills is underestimated, the MOC variability is well represented by a simple integrator of convection in the Irminger Sea, which fits better than a direct integration of NAO forcing.

1. Introduction

The North Atlantic Ocean is a key element of the earth's climate. The cyclonic circulation at depth along the boundaries, the deep western boundary current (DWBC), is the deep limb of the Atlantic meridional overturning circulation (MOC) that contributes substantially to the energy balance of the earth. The MOC is, indeed, associated with a poleward heat transport of about 1 PW (Petawatts = 10^{15} W) in the tropical North Atlantic, which is comparable to the atmospheric contribution at this latitude (Trenberth and Caron 2001). Fluctuations of the DWBC may induce changes in the poleward heat transport that would have a significant impact on the Atlantic–European climate (Vellinga and Wood 2002). The objective of this paper is to clarify the mechanisms of variability of the whole subpolar gyre, including its deep component, and its link with buoyancy and wind forcing over the North Atlantic.

A significant part of the variability of the oceanic circulation in the North Atlantic is driven by changes in the North Atlantic Oscillation (NAO), which is the dominant mode of atmospheric variability in the North Atlantic sector (Barnston and Livezey 1987). The NAO has exhibited substantial interannual variability during the last 50 yr, switching from mostly negative phases in the 1960s to strong and persistent positive phases in the 1970s, 1980s, and early 1990s, before decreasing in the mid-1990s. Observations reveal a decrease of the strength and a contraction of the subpolar gyre as the NAO switched from a positive to negative phase in the mid-1990s (Bersch 2002; Flatau et al. 2003; Häkkinen and Rhines 2004; Bersch et al. 2007). Curry and McCartney (2001) considered the potential energy anomalies derived from hydrographic measurements in the Labrador Basin as a proxy for the subpolar gyre strength. The changes were not directly covariant with the NAO but, to first order, the ocean signal seemed to

Corresponding author address: Julie Deshayes, WHOI MS#21, 266 Woods Hole Rd., Woods Hole, MA 02543.
E-mail: jdeshayes@whoi.edu

DOI: 10.1175/2008JCLI1882.1

reflect a time integration of the NAO forcing. They suggested that these changes were primarily influenced by dense water formation, which is in turn influenced by the NAO. Similarly, Häkkinen and Rhines (2004) suggested that the subpolar gyre weakening since 1995 was primarily due to the lack of dense water formation.

Realistic hindcast simulations with oceanic general circulation models (OGCMs) forced by observed atmospheric forcing shed light on the variability in the North Atlantic during the last 50 yr and help us to understand its link with atmospheric variability. Häkkinen (1999) reconstructed the variability of the meridional heat transport in the North Atlantic from 1951 to 1993, with an OGCM of moderate horizontal resolution (about 1°), emphasizing the correlation between the MOC and oceanic heat loss in the North Atlantic, via dense water formation, on both interannual and longer time scales. Wind stress forcing over the North Atlantic also drives the subpolar gyre and the MOC, as suggested by Eden and Willebrand (2001) in similar simulations with idealized forcing. The ocean response to wind forcing associated with a positive NAO phase consisted of a fast barotropic anticyclonic circulation anomaly near the subpolar front followed by a baroclinic adjustment, which lead to an increase in the subpolar gyre strength and the MOC 3 yr after the positive NAO phase. Hence both wind and buoyancy forcing seem to play a role in the oceanic response to changes in the NAO.

Eden and Willebrand (2001) describe the oceanic response to NAO-related buoyancy forcing as a baroclinic boundary wavelike structure, traveling southward to midlatitude, which induced an enhanced MOC 2–3 yr after convection occurred. Although Bentsen et al. (2004) discussed a similar southward propagation of anomalies induced by dense water formation in the Labrador Sea in a different OGCM, this mechanism is not visible in the simulation studied by Gulev et al. (2003). They suggested instead that convection influences the subpolar gyre circulation via a geostrophic adjustment to changes in interior stratification. While the studies mentioned above used simulations of rather coarse resolution (about 1°), Böning et al. (2006) considered simulations of the circulation in the North Atlantic of higher resolution (⅓° and 1/12°). In these simulations, convection induced fast boundary wave processes followed by advective spreading of newly formed water masses.

We described the same mechanism for the influence of convection on the DWBC in a simulation based on the same OGCM as Bentsen et al. (2004) but with 4 times higher resolution (20 km; Deshayes et al. 2007, hereafter DFD). However we emphasize that this fast connection between dense water formation and the circulation only exists when convection occurs close to the boundary currents, namely in the Irminger Sea in this simulation. In the Labrador Sea, dense water is formed in the interior of the basin where it tends to accumulate and recirculate, a reservoir effect that is consistent with observations (Straneo et al. 2003; Kvaleberg and Haine 2006), and hence has less influence on the surrounding boundary currents. The objective of this paper is to investigate whether the Irminger and Labrador Seas play a different role in the North Atlantic response to atmospheric forcing.

The hindcast simulation of the North Atlantic from 1953 to 2003 used in this study is presented in section 2. Variability in the wind and buoyancy forcing, and their connection with the NAO, is presented in section 3. We then discuss the variability of the circulation in the subpolar gyre and the MOC, and their link with atmospheric forcing and dense water formation (section 4). Conclusions are given in section 5.

2. The simulation

The model is the Nansen Center version (Bentsen et al. 2004; Drange et al. 2005) of the Miami Isopycnic Coordinate Ocean Model (MICOM; Bleck et al. 1992) in a regional configuration of the North Atlantic from 30° to 78°N with 20-km horizontal resolution. To reproduce the influence of the global oceanic circulation (this is particularly important for the subtropical gyre, which is *cut* at 30°N), the regional model is relaxed toward a global 40-km version of the same model by means of one-way nesting along its lateral boundaries. The global model fields are read once a week and interpolated to specify the relaxation boundary conditions for the regional model at each time step.

The model is isopycnal (vertical levels are surfaces of constant density) and has 26 density layers. The upper layer represents a vertically uniform mixed layer with variable temperature and salinity, hence density. The 25 layers below have constant potential density but variable thickness and temperature. The simulated salinity is diagnosed based on the simplified equation of state by Friedrich and Levitus (1972). Sea ice dynamics and thermodynamics are represented by the model of Harder (1996) and Drange and Simonsen (1996). The isopycnal diffusivity for layer interface, momentum, and tracer dispersion is 400 $m^2 s^{-1}$, 500 $m^2 s^{-1}$, and 300 $m^2 s^{-1}$, respectively. These relatively high values compensate for the lack of mesoscale eddies in the subpolar gyre due to the limited horizontal resolution. In the subtropics, horizontal resolution is sufficient to allow for mesoscale eddies, but they are heavily damped by the Laplacian isopycnal diffusivity used in the model

(Willebrand et al. 2001). Diapycnal mixing is parameterized as a function of stratification $K_d = 3 \times 10^7 N^{-1}$ $m^2 s^{-1}$, where N is the Brunt–Väisälä frequency.

The global model was spun up for 85 yr by applying monthly climatological (for 30 yr) then daily (from 1948 to 2003) National Centers for Environmental Prediction–National Center for Atmospheric Research (NCEP–NCAR) reanalysis fields (Kalnay et al. 1996), using the scheme of Bentsen and Drange (2000) that recalculates the latent and sensible heat fluxes based on the simulated oceanic conditions. The spinup integration was also used to define a correction flux for salinity applied afterward in both the global and the regional simulations. The global simulation at the end of the spinup was interpolated and used as the initial condition for the regional simulation. The regional and the global simulations were then both forced with the daily mean NCEP–NCAR reanalysis fields from 1948 to 2003. In the regional model only, the mixed layer temperature and salinity fields were linearly relaxed toward the monthly mean climatological values of Levitus and Boyer (1994) and Levitus et al. (1994), respectively. The relaxation scheme has been shown to be sufficiently weak to allow for realistic seasonal-to-interannual variations in the simulated hydrography in the northern North Atlantic (Hátún et al. 2005).

The circulation in the North Atlantic corresponds well to the observations (Lavender et al. 2000; Reverdin et al. 2003), besides the overshoot of the Gulf Stream that remains close to the topography up to 45°N, due to the limited horizontal resolution (Fig. 1). In the subpolar gyre, the boundary currents feature a decrease of amplitude with increasing depth but only little change of direction, as illustrated along two sections in Fig. 2 (see location of the sections in Fig. 1). A recirculation cell occupies the interior of the basins, with current going northwestward along the Labrador Current, then northeastward at 55°N, 48°W, from where it either turns west toward the interior of the Labrador Sea or east toward the interior of the Irminger Sea. This cell has been identified in drifters (Lavender et al. 2000) and chlorofluorocarbon (CFC) data (Talley and McCartney 1982). In this simulation, the transport of dense water across the Greenland–Scotland Ridge is about three times smaller than observed (Dickson and Brown 1994), so that the influence of water masses coming from the Nordic seas on the subpolar gyre circulation and the MOC is underestimated.

The interior of the Labrador and Irminger Seas is on average 1°–2°C colder and 0.3 fresher than observed climatologies (Levitus and Boyer 1994; Levitus et al. 1994), presumably because of the too-weak turbulent mixing that reduces the influence of the warm and salty water advected by the boundary currents. Because the mixed layer is vertically homogeneous in an isopycnic model, baroclinic instability is limited (Eldevik 2002) and restratification is too weak (Rousset et al. 2007, manuscript submitted to *Ocean Modell.*), which may also contribute to the cold and fresh biases. Although there are biases in the mean temperature and salinity distributions, this may not influence their variability as the salinity anomalies in the subpolar gyre are similar to those extracted from observations after the end of the 1960s (Curry and Mauritzen 2005) except below 2500 m, presumably because of a drift in the simulation. This will be discussed elsewhere.

3. Variability of the atmospheric forcing in the North Atlantic

Atmospheric variability in the North Atlantic and its close relationship with the NAO has been largely discussed in previous studies (see Marshall et al. 2001a for a review). We only rapidly outline in this section the variability in buoyancy and momentum fluxes to the subpolar gyre and their connection with the NAO.

In the subpolar gyre, the thermal contribution to density fluxes is at least one order of magnitude larger than the haline contribution (Schmitt et al. 1989). This suggests that the heat fluxes alone may be used to a good approximation to describe the variability of the surface buoyancy fluxes. The heat fluxes used to force the model were calculated by applying bulk formulas based on the surface atmospheric conditions extracted from the NCEP–NCAR reanalysis data and the actual simulated sea surface temperature (Bentsen and Drange 2000). Because these fluxes are not available any more, we use the (presumably largely similar) surface heat fluxes from the NCEP–NCAR reanalyses directly when estimating their link with the oceanic variability. The total heat flux into the ocean (sensible and latent heat fluxes, plus short- and longwave radiation) is strongly negative in winter, from December to March, when the ocean heats the atmosphere, most importantly near the Gulf Stream and in the Labrador Sea. The main mode of interannual variability of the winter heat fluxes, as described by the first empirical orthogonal function (EOF) in Fig. 3 (top) is, in this polarity, negative over most of the subpolar gyre and minimum in the center of the Labrador Sea where deep convection occurs. The associated principal component (PC; Fig. 4, black dashed line) shows that the heat loss was maximum in 1972, in the mid-1980s, and the early 1990s, which corresponds to the simulated (DFD) and observed (Dickson et al. 1996; Yashayaev 2007) events

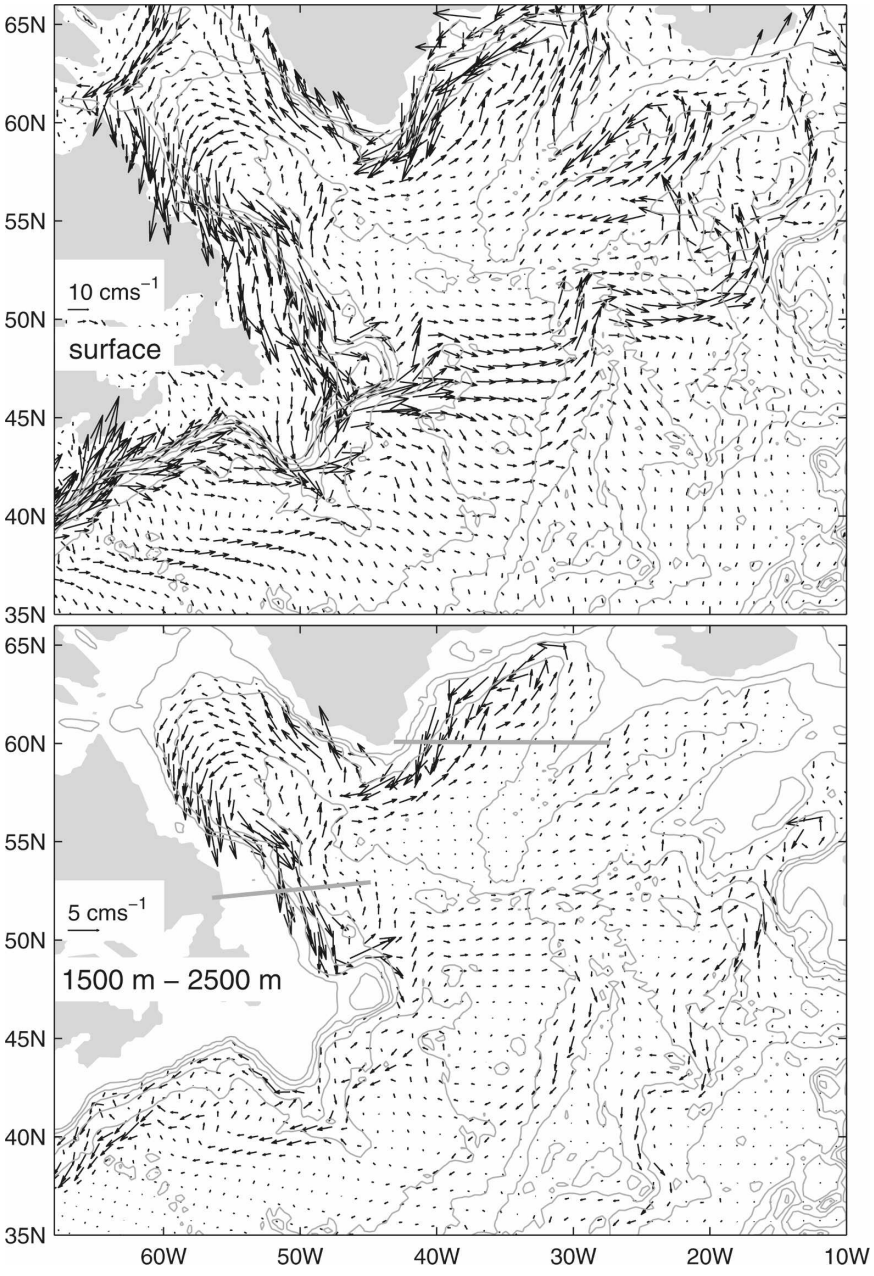

FIG. 1. Mean circulation in the North Atlantic (top) at the surface and (bottom) averaged between 1500 and 2500 m (only one vector every 9 grid cells is shown). Thin gray lines indicate bathymetry contours (from 500-m depth, contour interval: 1000 m), while thick straight lines indicate the location of sections 60° and 52°N.

of deep water formation in the Labrador Sea. There is also a good correlation ($r = 0.74$) with the yearly NAO index, defined here as the yearly average of PC1 of monthly anomalies in sea level pressure over the North Atlantic (Fig. 4, thick gray line). Note that the EOF in Fig. 3 is influenced by the presence of sea ice in the Labrador Sea and its significant interannual variability (Deser et al. 2002). However, when applying a mask corresponding to the maximum sea ice extent over the Labrador Sea, Gulev et al. (2007) obtain a similar spatial pattern for the first EOF of the net heat flux anomalies in the North Atlantic.

Ekman pumping is most intense in winter, from November to March, and positive north of 50°N, inducing a doming of the isopycnals and a strong cyclonic circulation around the Irminger and Labrador Seas (Spall

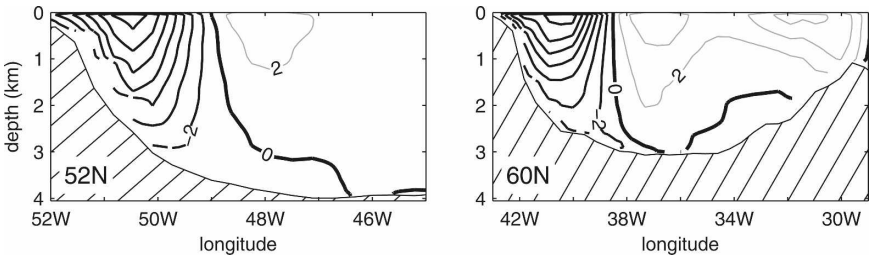

FIG. 2. Mean circulation across sections (left) 52°N and (right) 60°N, with gray lines for northward current, thin black lines for southward current, and thick black lines for 0 contours (contour interval: 2 cm^{-1}).

and Pickart 2003). Fluctuations of the Ekman pumping are dominated by the natural variability of the atmosphere, which has an approximately white frequency spectrum. Hence we use the yearly averages to discuss its interannual variability. The first mode of Ekman pumping variability in Fig. 3 (bottom) represents, in this polarity, a northward migration of the zero wind stress curl line to about 58°N. Note that a positive NAO phase induces positive (respectively negative) Ekman pumping anomalies in the northern (southern) part of the Labrador Sea. The associated PC is maximum in the mid-1970s, the mid-1980s, and the early 1990s (Fig. 4, black plain line), and is well correlated with the yearly NAO index ($r = 0.85$).

In the following section, we thus use the yearly NAO index as a reference for the interannual variability of atmospheric forcing in the North Atlantic. On the monthly time scale, a positive NAO phase is also characterized by intensified heat loss in the subpolar gyre, especially in the Labrador Sea, positive anomalies in Ekman pumping in the northern subpolar gyre, and negative Ekman pumping anomalies in the southern subpolar gyre, similar to the respective EOFs shown above.

4. Oceanic variability

Because of the vertical structure of the mean currents, the circulation in the subpolar gyre is well described by the barotropic streamfunction (BTSF) derived from the vertically integrated currents. The mean barotropic streamfunction is maximum in the Labrador Sea and in the Irminger Sea (Fig. 5, top left). The mean intensity of the subpolar gyre south of Cape Farewell is 40 Sv (1 Sv $\equiv 10^6$ m^3 s^{-1}), comparable with observations that range from 34 to 40 Sv (Clarke 1984; Reynaud et al. 1995) and with similar OGCM simulations (Treguier et al. 2005, their Fig. 5). The recirculation cell that goes from the Labrador Sea to the Irminger Sea clearly appears in the center of the subpolar gyre, consistent with the observed geostrophic pressure at 700-m depth (Lavender et al. 2000). The circulation in the subtropical gyre is strongly underestimated, however, in part because it is affected by the southern boundary of the regional model at 30°N.

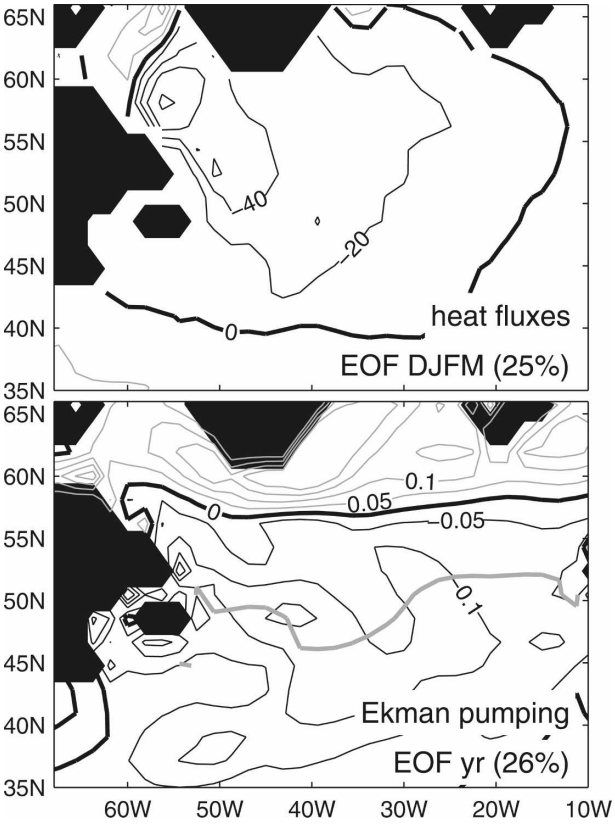

FIG. 3. (top) EOF1 of the winter averages of the surface heat fluxes (anomalies in W m^{-2}; gray lines for positive, i.e., downward, anomalies; thin black lines for negative anomalies; thick black line for 0 contour). (bottom) EOF1 of the yearly Ekman pumping (anomalies in 10^{-6} m s^{-1}; gray lines for positive anomalies inducing a doming of the isopycnals at depth; thin black lines for negative anomalies; thick black lines for 0 contours). The yearly mean zero Ekman pumping isoline at 50°N is indicated by the thick gray line and the percentage of represented variance indicated.

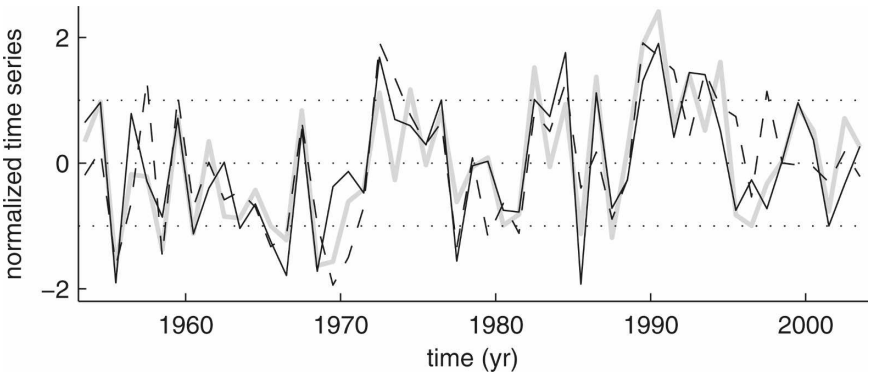

FIG. 4. Normalized time series of the yearly NAO index (thick gray line), PC1 of the winter heat fluxes (dashed black line), and PC1 of the yearly Ekman pumping (plain black line).

The MOC, defined as the zonally averaged meridional circulation, is calculated after interpolation of the monthly isopycnal velocities on levels of fixed depth (with vertical resolution of 50 m). The mean MOC in the North Atlantic is maximum at 44°N and equals 11 Sv (Fig. 5, top right), which is less than the 15 Sv estimated from hydrographic observations (Ganachaud and Wunsch 2000), in part because of the underestimation of the dense water transport across the Greenland–Scotland sills. Nevertheless it is comparable with other OGCM simulations, which mean MOC ranges from 10 to 23 Sv (Häkkinen 1999; Gulev et al. 2003; Haak et al. 2003; Bentsen et al. 2004; Böning et al. 2006).

The circulation in the subpolar gyre varies on a broad range of time scales. In this paper, we primarily focus on the interannual-to-decadal variability. Hence a linear trend has been removed from all time series before calculating the regressions and correlations. However, the trends are not removed when displaying the time series. As the NAO is the dominant mode of atmospheric variability in the North Atlantic, it has a major imprint on the oceanic variability. To begin with, we briefly describe the monthly variability of the circulation driven by the NAO.

a. Monthly variability

The regression of the monthly anomalies of the BTSF on the NAO index shows negative (i.e., cyclonic) anomalies north of 58°N and positive (anticyclonic) anomalies south of it (Fig. 5, middle), suggesting a decrease of the circulation in the Labrador Sea and an increase of that in the Irminger Sea when the NAO is in a positive phase. The circulation nearly follows the f/H contours, except seaward of the Grand Banks, where the BTSF positive anomalies clearly cross the f/H isolines (not shown), reflecting the wind stress curl forcing (Fig. 3). The response is consistent with the anticyclonic intergyre gyre described by Marshall et al. (2001b). The regression of the monthly anomalies of the MOC on the NAO index shows a decrease of the MOC at high latitude together with an increase at midlatitude, with anomalous downwelling near 40°N, which is again consistent with a rapid adjustment to the Ekman transport and pumping.

b. Interannual-to-decadal variability

The interannual variability of the circulation is first described by an EOF analysis of the yearly averaged data. The first mode of variability of both the BTSF and the MOC explains a large fraction of the variance, as much as 74% for the MOC, and resembles the mean circulation (Fig. 5, bottom), thus describing a modulation of its strength. The PCs indicate an intensification of both the BTSF and the MOC since the mid-1970s, with peaks in the mid-1980s and the early 1990s and a decrease thereafter (Fig. 6). The time variability of the BTSF is consistent with the estimate of Belkin (2004) and with altimetry data in the 1990s (Häkkinen and Rhines 2004). The simulated variability of the MOC is similar to that seen in most OGCM simulations (e.g., Häkkinen 1999; Gulev et al. 2003; de Coëtlogon et al. 2006; Böning et al. 2006). Its power spectrum broadly behaves as ω^{-2} at interannual frequencies and flattens at periods longer than about 20 yr (Fig. 7), indicating that the main mode of MOC variability has maximum variance at decadal periods.

Correlation of the BTSF and MOC PCs with the yearly NAO index reveals that both circulations intensify 2 yr after a positive NAO phase (Fig. 8, top). PC1 of the BTSF is also correlated in phase with the yearly NAO index, reflecting the fast intensification of the northern subpolar gyre driven by NAO-related Ekman pumping as described above. Note that the southern boundary of the model at 30°N dampens the variability

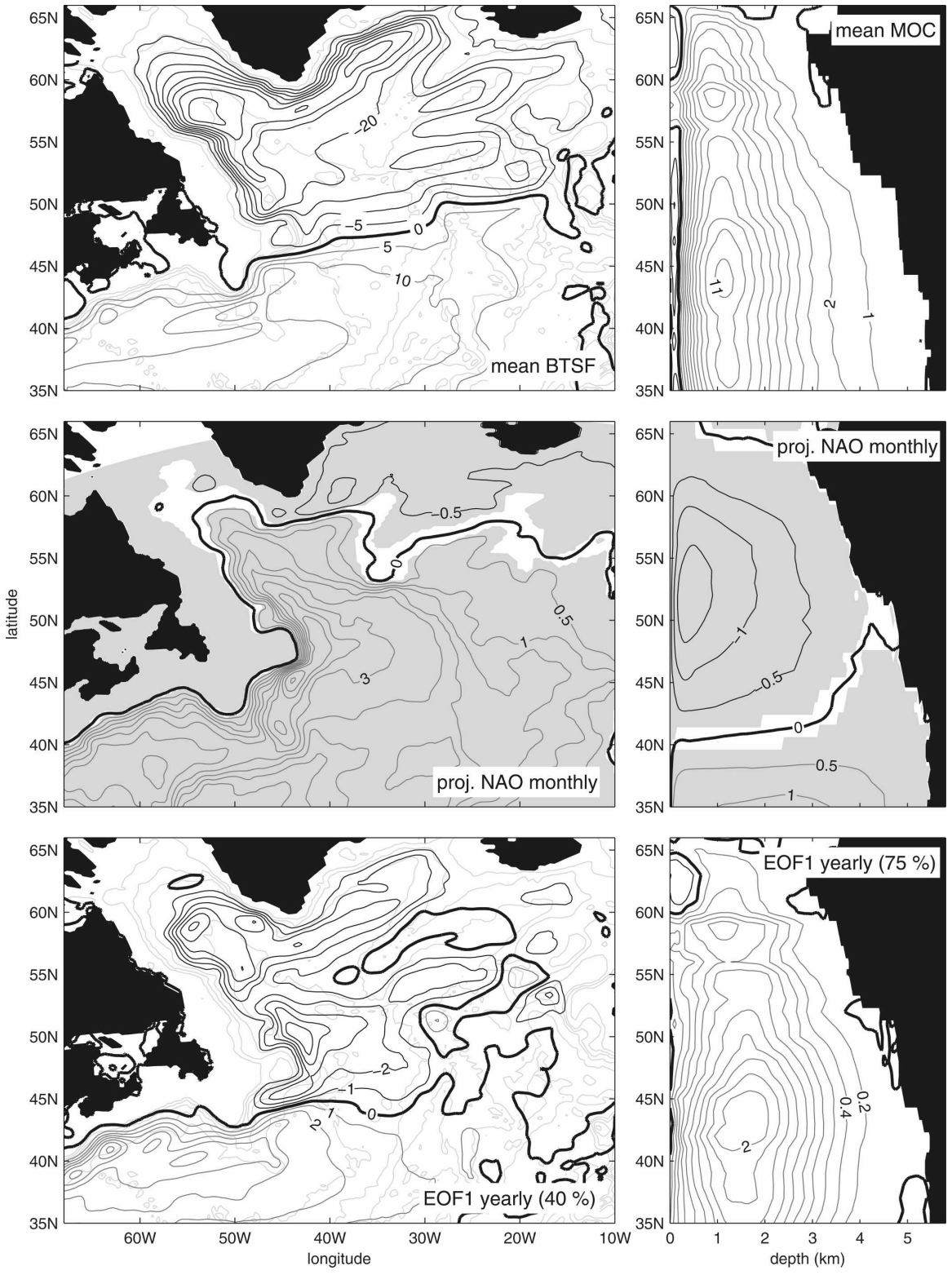

FIG. 5. (top left) BTSF and (top right) MOC (both in Sv), (middle) mean monthly anomalies projected on the NAO index, and (bottom) EOF1 of the yearly data. Dark gray lines stand for positive anomalies (i.e., clockwise circulation), thin black lines for negative ones, and thick black lines for 0 contours. Gray shading in middle panels indicates where the monthly anomalies are significantly correlated with the NAO index. Light gray contours on left panels indicate bathymetry (contour interval: 1000 m from 500-m depth).

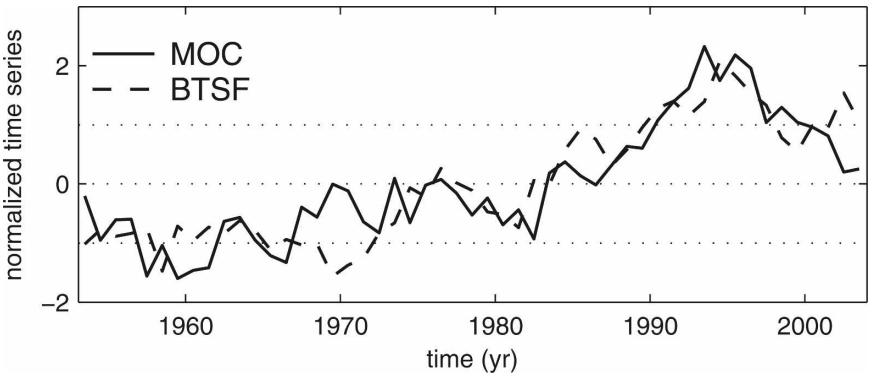

FIG. 6. PC1 of yearly MOC (plain line) and BTSF (dashed line).

of the subtropical gyre, despite the restoring to the global simulation. However, the interannual-to-decadal variability of the subpolar gyre, which we are interested in, does not seem to be affected.

The regression of the MOC on the yearly NAO index resembles the fast adjustment to Ekman pumping (Fig. 9, top). When the NAO leads by 1 yr, the MOC anomalies change sign and feature an intensification of the MOC at high latitude, which extends southward when the NAO leads by 2 yr and more (Fig. 9, bottom panels). This indicates that the intensification of the baroclinic circulation after a positive NAO phase starts in the northern subpolar gyre. Similarly, the regression of the BTSF on the yearly NAO index resembles the fast adjustment to Ekman pumping (Fig. 10, top left), with negative anomalies only in the Irminger Sea. These anomalies increase and extend southwestward to the Labrador Sea when the NAO leads by 1 yr and more (Fig. 10, other panels). Because EOFs describe standing patterns, a single one cannot reflect propagating anomalies. Hence, we show in Fig. 11 the first EOF of the BTSF calculated separately for the Labrador and Irminger Seas. Correlation of the associated PCs with the NAO index (bottom right) confirms that the gyre circulation intensifies in the Irminger Sea 1 yr after a positive phase of the NAO, while in the Labrador Sea it only intensifies 1 or 2 yr later. It is important to mention that the results presented above for the high- and low-frequency variability of the circulation have already been shown in previous studies, but this phase lag has never been noted or investigated. To identify the associated mechanisms, we consider the vertical structure of the circulation across sections at 52°N in

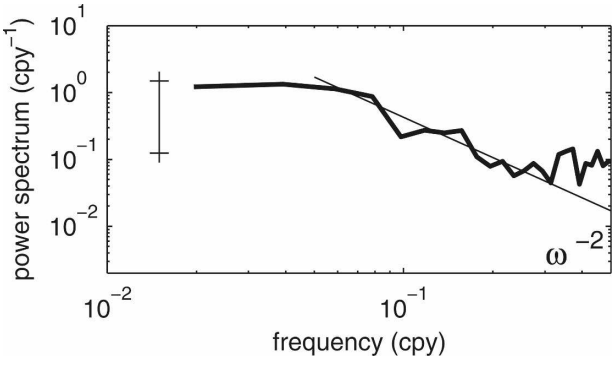

FIG. 7. Power spectrum of MOC PC 1 calculated with the multitaper method using three windows. The 95% confidence interval is given. Thin line indicates ω^{-2} power law.

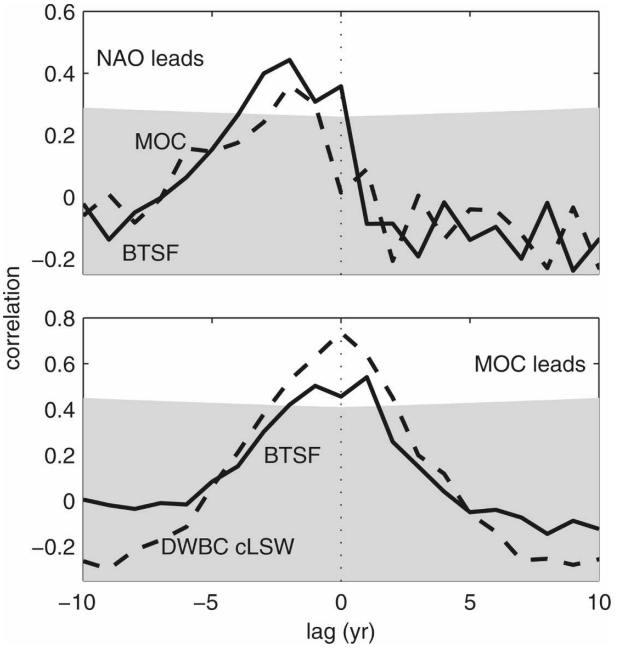

FIG. 8. (top) Correlation between the NAO index and PC1 of MOC (dashed line) and BTSF (plain line), the NAO index leads for negative lags. (bottom) Correlation between MOC PC1 and BTSF PC1 (plain line) and with the transport of cLSW in the DWBC (dashed line), MOC PC1 leads for positive lags. Shading indicates 5% significance levels.

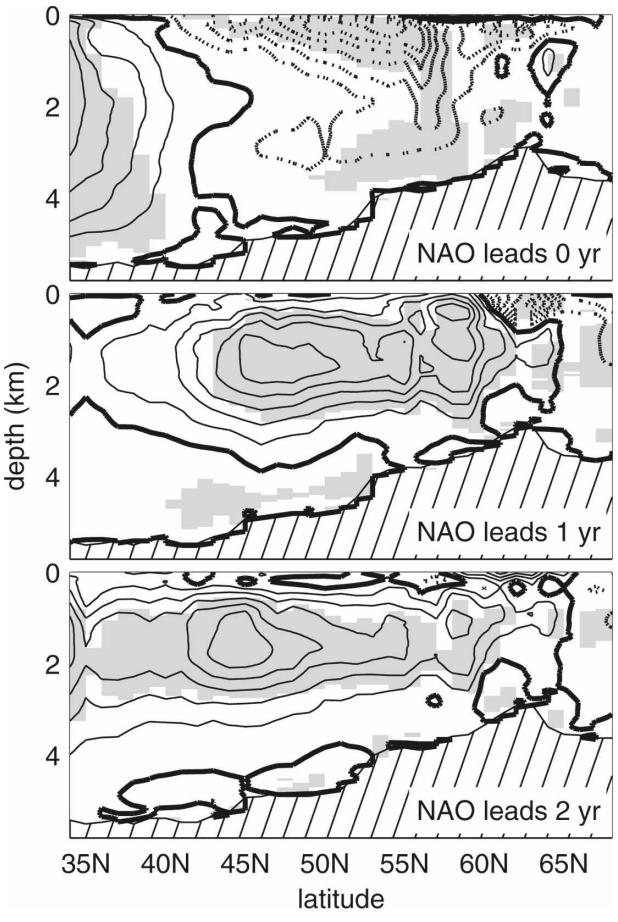

FIG. 9. Regression of the yearly averages of the MOC on the annual NAO index (contour interval 0.1 Sv, plain lines for positive covariance, dotted lines for negative, thick lines for 0). Shading indicates 5% significance levels.

the Labrador Sea and at 60°N in the Irminger Sea (see location in Fig. 1).

During a positive NAO phase, there are northward anomalies in the Labrador Current, consistent with the fast barotropic adjustment to the negative anomalies in Ekman pumping in the southern subpolar gyre (Fig. 12, left). One year later, an intensification of the deep southward Labrador Current appears from 1500- to 3000-m depth, while northward anomalies are still visible above, albeit with a weaker intensity. According to DFD, the transport of dense water by the deep Labrador Current increases 0–2 yr after convection occurs in the Labrador and Irminger Seas, convection lagging a positive NAO phase by 0–1 yr. This intensification is likely to be first due to the propagation of topographic waves and then the advection of the newly formed dense water, consistent with Häkkinen (1999), Eden and Willebrand (2001), Bentsen et al. (2004), and Böning et al. (2006).

Surface anomalies in the Labrador Current change sign 2 yr after a positive NAO phase, presumably because of the strong buoyancy loss in the Labrador Sea and baroclinic adjustment to the enhanced Ekman pumping in the northern subpolar gyre (see Fig. 3). It may also be due to a barotropization of the deep southward anomalies resulting from the interaction between the steep topography and the stratification at depth (Lazier and Wright 1993; Hallberg and Rhines 1996). Which mechanism dominates could only be established by sensitivity experiments. The southward boundary current reaches its peak 3 yr after the positive NAO phase, affecting the whole water column, and the current anomalies decrease thereafter. Hence, the intensification of the cyclonic circulation in the Labrador Sea, driven by dense water formation, surface cooling, and Ekman pumping in the northern subpolar gyre, is somewhat delayed by the barotropic response to Ekman pumping in the southern subpolar gyre that first decreases the Labrador Current.

In the Irminger Sea, the intensification of the circulation after a positive NAO phase is more straightforward, as positive Ekman pumping anomalies and dense water formation act in the same fashion. The regression of the current anomalies on the NAO index indicates a weak but significant intensification of the East Greenland Current during a positive NAO phase (Fig. 12, right), presumably due to the barotropic adjustment to Ekman pumping. The intensification is strongest when the NAO leads by 1–2 yr, while current anomalies develop in the eastern part of the basin. The same current anomalies are significant in the regression on the index of convection in the Irminger Sea (defined as the normalized mixed layer volume in the area of convection), but with a much larger amplitude (not shown). The current changes during events of convection are associated with a substantial doming of the isopycnals in the center of the Irminger Sea, which intensifies the boundary cyclonic circulation (Fig. 13). It also induces an eastward migration of the Irminger Current above the Reykjanes Ridge, 0–1 yr after a positive phase of the NAO, consistent with observations (Flatau et al. 2003). Hence, the intensification of the cyclonic circulation in the Irminger Sea is driven by the coherent influence of Ekman pumping and dense water formation, and it rapidly takes place after a positive phase of the NAO. It is important to note that in this simulation, convection in the Irminger Sea occurs too close to the northern boundary current, resulting in a rapid flushing of the newly formed dense water (DFD). Hence, the influence of convection on the surrounding boundary currents is probably too rapid and overestimated.

The intensification of the circulation in the Irminger

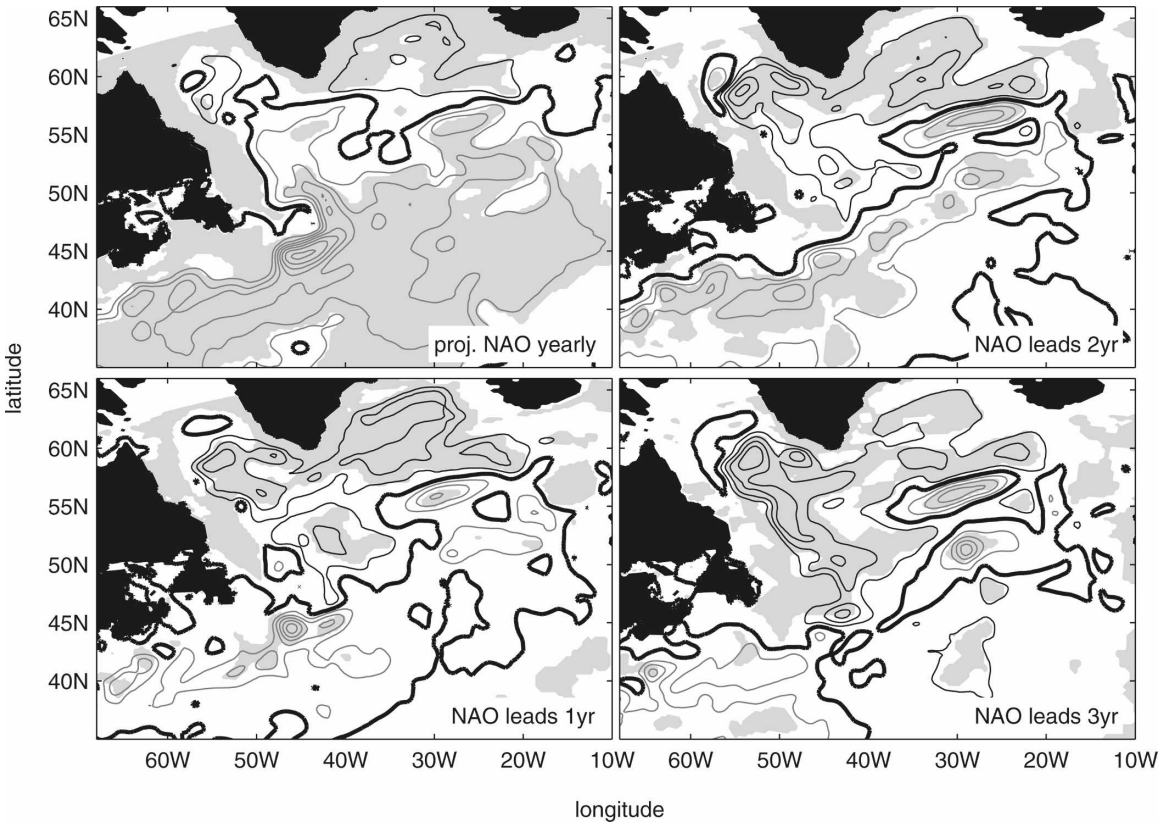

FIG. 10. Regression of the yearly averages of the BTSF on the annual NAO index (contour interval 0.5 Sv, thin black lines for negative covariance, gray lines for positive, thick lines for 0). Shading indicates 5% significance levels.

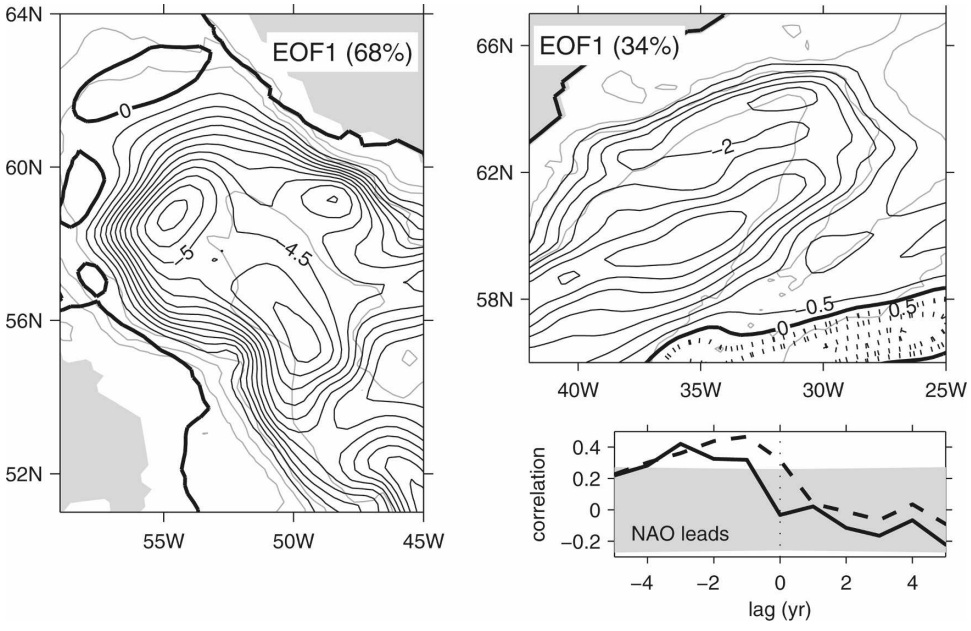

FIG. 11. EOF1 of the BTSF in the (left) Labrador and (top right) Irminger Seas from yearly averages (contour interval 0.5 Sv, dotted lines for positive contours, plain lines for negative ones, thick line for 0). (bottom right) Correlation of the associated PCs (plain line for the Labrador Sea, dashed line for the Irminger Sea) with the NAO index, which leads for negative lags. Shading indicates the 5% significance level.

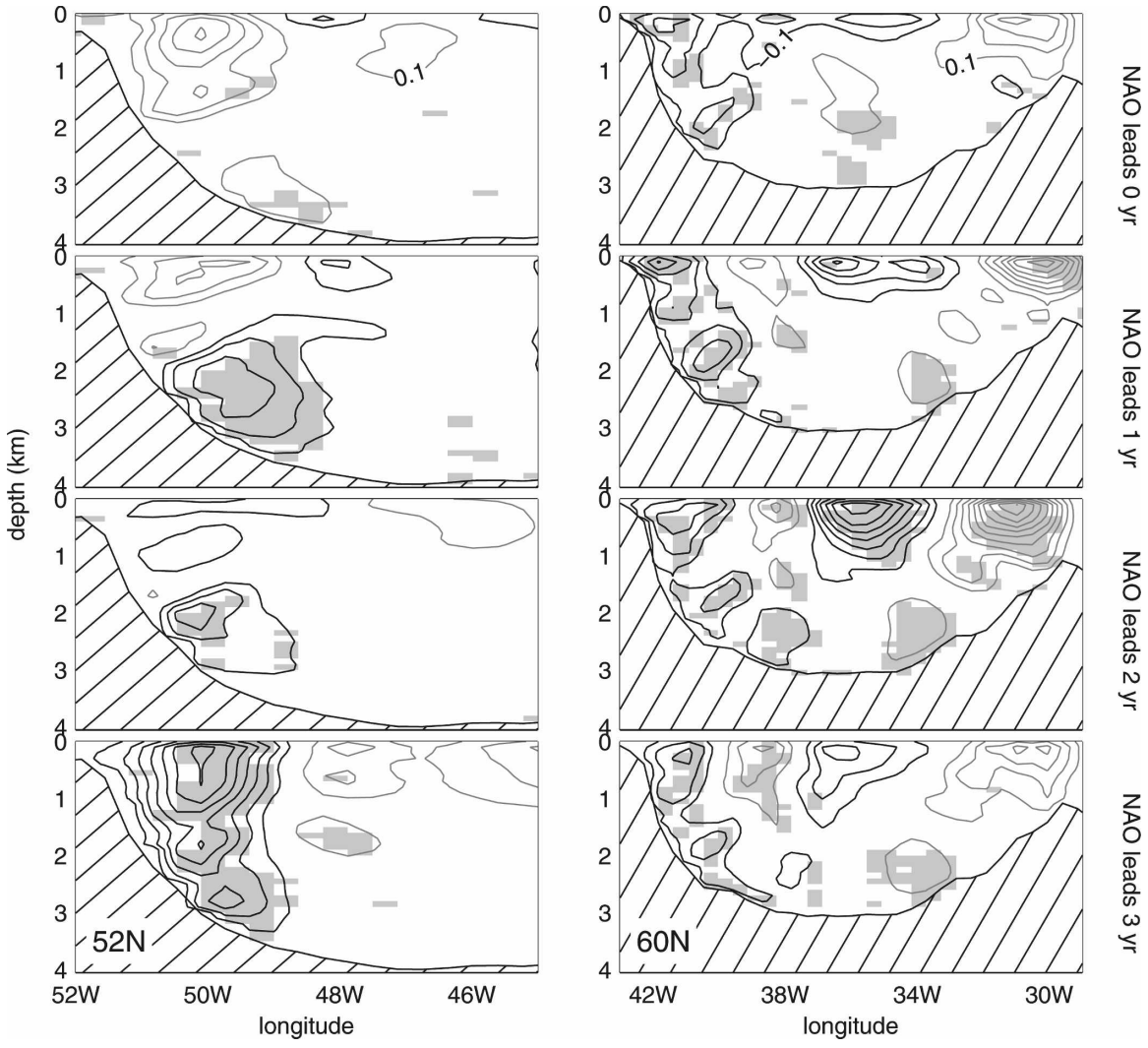

FIG. 12. Regression of the current across sections (left) 52°N and (right) 60°N on the yearly NAO index, (top) in phase and (others) when the NAO leads by 1–3 yr. Gray shading indicates where the current anomalies are significantly correlated with the NAO index. Positive anomalies (northward) are drawn in dark gray, negative anomalies (southward) in black (contour interval: 0.1 cm^{-1}), 0 contour is omitted.

and Labrador Seas contributes to the intensification of the MOC via the DWBC, whose transport of classical Labrador Sea Water (cLSW) is highly correlated with PC1 of the MOC (Fig. 8, bottom). PC1 of the BTSF is also well correlated with PC1 of the MOC, although the correlation is maximum when the MOC (and the DWBC) leads by 1 yr. This is probably due to the adjustment of the circulation in the Labrador Sea, where the circulation at depth tends to lead its surface counterpart.

5. Conclusions and discussion

A hindcast simulation of the North Atlantic from 1953 to 2003 has been used to investigate the variability of the circulation in the subpolar gyre and its link with atmospheric forcing, which is dominated by the NAO. The simulated subpolar gyre and the MOC intensified in the early 1970s, in the mid-1980s and peaked in the early 1990s, which corresponds to the periods of positive NAO phase, and then decreased.

During a positive phase of the NAO, the Ekman pumping anomalies are positive (i.e., inducing a doming of the isopycnals at depth) in the northern subpolar gyre but negative in the southern subpolar gyre, in particular over the Labrador Current. They rapidly generate an anticyclonic barotropic response (strongly influenced by topography) in the southern subpolar gyre and a cyclonic one in the northern subpolar gyre, consistent with the intergyre gyre described by Marshall et

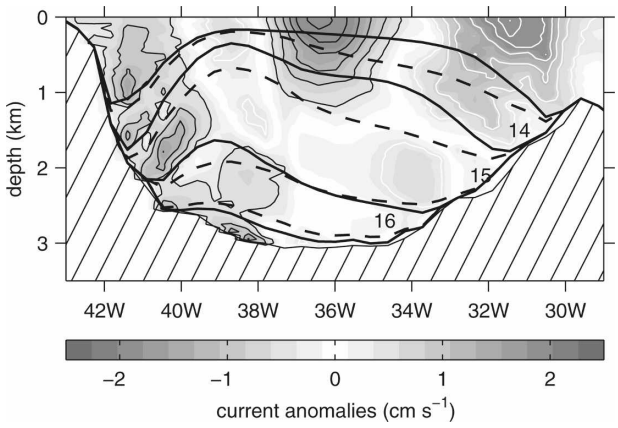

FIG. 13. Position of layers 14 (σ_0 = 27.71 kg m^{-3}), 15 (σ_0 = 27.77 kg m^{-3}), and 16 (σ_0 = 27.82 kg m^{-3}) during the years of deep convection in the Irminger Sea (thick plain lines) and on average from 1953 to 2003 (thick dashed lines), and meridional current anomalies during the years of deep convection (gray shading and white thin contours for positive, i.e., northward, anomalies; black thin contours for negative anomalies; contour interval: 0.5 cm^{-1}).

al. (2001b). The cyclonic subpolar gyre circulation thus rapidly decreases in the south and increases in the north. The intensification of the northern subpolar gyre is reinforced by an adjustment to the intensified buoyancy loss and dense water formation in the Irminger Sea, where the cyclonic circulation is most intense 1–2 yr after a positive NAO phase. Dense water formation also occurs in the Labrador Sea, but because of the early decrease of the southern subpolar gyre strength, the intensification of the equivalent barotropic (whose direction is uniform and amplitude decreasing with depth) cyclonic circulation is delayed. The Labrador Current presents barotropic northward anomalies when the NAO is in a positive phase. One year later, southward anomalies appear at depth, while the anomalies above remain northward. This peculiar vertical structure of the current anomalies suggests that they are induced by dense water formation rather than reflecting an upper-ocean adjustment to wind or buoyancy forcing. The surface anomalies in the Labrador Current eventually change sign, presumably because of buoyancy loss over the basin and baroclinic adjustment to the Ekman suction in the northern subpolar gyre, as well as a coupling between the surface and deep current anomalies. The cyclonic circulation in the Labrador Sea only peaks 3 yr after a positive NAO phase, thus lagging that of the northern subpolar gyre.

In this simulation, the MOC is directly driven by changes in the DWBC, and the transport of cLSW in the DWBC is mostly influenced by convection in the Irminger Sea (DFD). The MOC intensifies 2 yr after a positive NAO phase, and somehow leads the intensification of the gyre circulation in the Labrador Sea where the intensification first appears at depth, driven by dense water formation.

The intensification of the subpolar gyre and the MOC 2 yr after a positive phase of the NAO is consistent with previous studies, although the phase lag varies from 2 (Häkkinen 1999) to 3 yr (Eden and Willebrand 2001; Gulev et al. 2003). In these OGCMs, dense water formation occurs in the Labrador Sea. However, convection also occurs in the Irminger Sea in the simulation of Bentsen et al. (2004), based on the same OGCM as in this study but with a lower resolution, and it also has an influence on the MOC. An influence of Irminger Sea convection on the subpolar gyre has also been found in simulation ATL6 of Treguier et al. 2005 (their Fig. 7b), based on a different OGCM. However, the latter overestimates the mixed layer depth in the Labrador and Irminger Seas, illustrating that even high-resolution models have difficulties when trying to simulate realistic water mass characteristics and convection depth. A reviewer of this paper has suggested that our results are largely due to a model artifact of too strong convection in the Irminger Sea. Recent observations confirm that dense water formation occurred in the Irminger Sea (Falina et al. 2007), but in this model convection in the Irminger Sea occurs too close to the boundary current, and it may be too intense (DFD). This probably overestimates its influence on the surrounding circulation and may be responsible for the relatively fast adjustment of the MOC to convection. Yet we believe that it does not significantly impair our conclusion that the Irminger Sea convection has a strong impact on the interannual-to-decadal variability of the MOC. That the Labrador Sea convection only has a small influence on the circulation in the North Atlantic subpolar gyre is also suggested by observations (Pickart and Spall 2007).

In the spirit of Curry and McCartney (2001), we have reconstructed the MOC index with a first-order Markov process forced by the yearly NAO index. As the NAO spectrum is white, this basically assumes that the MOC responds to the stochastic NAO forcing as an integrator. The damping factor in the AR-1 model sets the dominant time scale of the MOC response and represents complex dissipation and feedback processes. Lacking knowledge of the latter, we have estimated the damping factor empirically by fitting an AR-1 spectrum to the MOC spectrum in Fig. 7. This yields a damping factor of (1/2.7) yr^{-1}. The reconstructed MOC time series (Fig. 14, dashed gray line) shows that the MOC can be coarsely considered as an integrator of NAO-related atmospheric forcing. The correlation between MOC

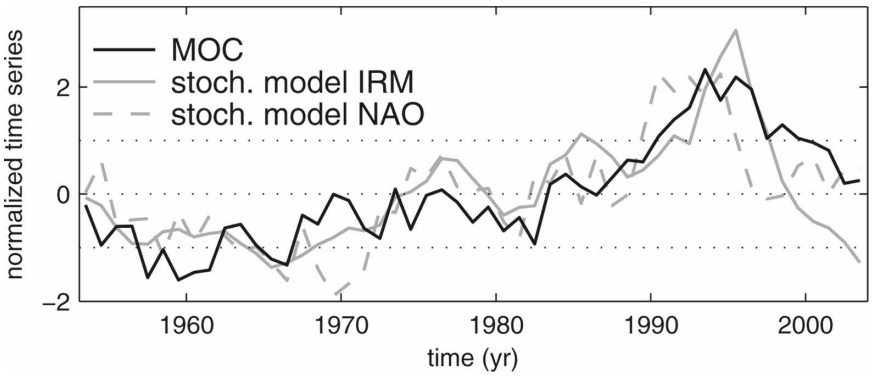

FIG. 14. MOC PC1 (black line) and a stochastic model forced by convection in the Irminger Sea (gray plain line) and by the yearly NAO index (gray dashed line).

PC1 and the stochastic model is 0.43, and 0.57 when the NAO leads by 1 yr. However, the correlation increases to 0.68 and is maximum without time lag when the stochastic model is forced by the time series of convection in the Irminger Sea (Fig. 14, plain gray line). The better agreement suggests that the MOC primarily behaves as an integrator of convection in the Irminger Sea. This is consistent with the heat flux integrator calculated by Häkkinen (1999) to reproduce the variability in meridional heat transport at 25°N, and it provides some support to the stochastic model of Deshayes and Frankignoul (2005).

The correlation between the reconstructed series and MOC PC1 increases when the time series are not detrended, reaching 0.68 and 0.76 at lag 0 and 1, respectively, in the case forced by the NAO, and 0.77 at lag 0 in that forced by the Irminger Sea convection. This suggests that, in the model, the connection between dense water formation, the NAO, and the MOC holds on the multidecadal time scale. However, the transport of dense water across the Greenland–Shetland sills is underestimated in the simulation, reducing the influence of convection in the Nordic seas. Since the latter may have a strong influence on the MOC at multidecadal-to-centennial scales (Beismann and Barnier 2004; Schweckendiek and Willebrand 2005), an extension of our results to longer time scales should be viewed with much caution.

It should be kept in mind that the link between dense water formation in the interior of a convective basin and the surrounding circulation is not well reproduced in non-eddy-resolving simulations. Higher-resolution idealized simulations indicate that the link is accomplished via turbulent mesoscale transfers of buoyancy between the interior and the boundary current (Spall 2004), which interact with the boundary current in a nonlinear way (Straneo 2006). In our relatively low-resolution simulation, the mesoscale turbulence is parameterized by a Laplacian isopycnal diffusivity, so that the adjustment time scale to the dense water formation may be poorly simulated. However, Böning et al. (2006) remarked that a realistic representation of the narrow boundary flows and the mesoscale eddies had little impact on the low-frequency variability of the subpolar gyre transport.

In this study, we have used linear statistical analysis to describe the variability of the circulation in the North Atlantic, suggesting that the bulk variability results from the ocean response to changes in the NAO. More sophisticated tools would be required to investigate the possible nonlinear effects associated with differences in the ocean response to a positive or a negative NAO phase, or the influence of atmospheric haline buoyancy forcing and other atmospheric modes of variability (Bojariu and Reverdin 2002; Josey and Marsh 2005).

Acknowledgments. We thank Hjálmar Hátún, Gilles Reverdin, Fritz Schott, and Anne-Marie Tréguier for stimulating discussions; Helge Drange for providing the OGCM data; and the two anonymous reviewers for their helpful comments. Support from the European FP6 project DYNAMITE (Contract 003903-GOCE) and (to CF) from the Institut Universitaire de France and NSF Grant 82677800 with the Woods Hole Oceanographic Institution is gratefully acknowledged.

REFERENCES

Barnston, A. G., and R. E. Livezey, 1987: Classification, seasonality and persistence of low-frequency atmospheric circulation patterns. *Mon. Wea. Rev.,* **115,** 1083–1126.

Beismann, J.-O., and B. Barnier, 2004: Variability of the meridional overturning circulation of the North Atlantic: Sensitivity to overflows of dense water masses. *Ocean Dyn.,* **54,** 92–106.

Belkin, I. M., 2004: Propagation of the "Great Salinity Anomaly" of the 1990s around the northern North Atlantic. *Geophys. Res. Lett.,* **31,** L08306, doi:10.1029/2003GL019334.

Bentsen, M., and H. Drange, 2000: Parameterizing surface fluxes

in ocean models using the NCEP/NCAR reanalysis data. RegClim General Tech. Rep. 4, Norwegian Institute for Air Research, Kjeller, Norway, 149–158.

——, ——, T. Furevik, and T. Zhou, 2004: Simulated variability of the Atlantic meridional overturning circulation. *Climate Dyn.,* **22,** 701–720.

Bersch, M., 2002: North Atlantic Oscillation-induced changes of the upper layer circulation in the northern North Atlantic Ocean. *J. Geophys. Res.,* **107,** 3156, doi:10.1029/2001JC000901.

——, I. Yashayaev, and K. P. Koltermann, 2007: Recent changes of the thermohaline circulation in the subpolar North Atlantic. *Ocean Dyn.,* **57,** 223–235.

Bleck, R., C. Rooth, D. Hu, and L. T. Smith, 1992: Salinity-driven thermocline transients in a wind- and thermohaline-forced isopycnic coordinate model of the North Atlantic. *J. Phys. Oceanogr.,* **22,** 1486–1505.

Bojariu, R., and G. Reverdin, 2002: Large-scale variability modes of freshwater flux and precipitation over the Atlantic. *Climate Dyn.,* **18,** 369–381.

Böning, C. W., M. Scheinert, J. Dengg, A. Biastoch, and A. Funk, 2006: Decadal variability of subpolar gyre transport and its reverberation in the North Atlantic overturning. *Geophys. Res. Lett.,* **33,** L21S01, doi:10.1029/2006GL026906.

Clarke, R. A., 1984: Transport through the Cape Farewell-Flemish Cap section. *Rapp. P.-V. Reun. Cons. Int. Explor. Mer.,* **185,** 120–130.

Curry, R. G., and M. S. McCartney, 2001: Ocean gyre circulation changes associated with the North Atlantic Oscillation. *J. Phys. Oceanogr.,* **31,** 3374–3400.

——, and C. Mauritzen, 2005: Dilution of the northern North Atlantic Ocean in recent decades. *Science,* **308,** 1772–1774.

de Coëtlogon, G., C. Frankignoul, M. Bentsen, C. Delon, H. Haak, S. Masina, and A. Pardaens, 2006: Gulf Stream variability in five oceanic general circulation models. *J. Phys. Oceanogr.,* **36,** 2119–2135.

Deser, C., M. Holland, G. Reverdin, and M. Timlin, 2002: Decadal variations in Labrador Sea ice cover and North Atlantic sea surface temperatures. *J. Geophys. Res.,* **107,** 3035, doi:10.1029/2000JC000683.

Deshayes, J., and C. Frankignoul, 2005: Spectral characteristics of the response of the meridional overturning circulation to deep water formation. *J. Phys. Oceanogr.,* **35,** 1813–1825.

——, ——, and H. Drange, 2007: Formation and export of deep water in the Labrador and Irminger Seas in a GCM. *Deep-Sea Res. I,* **54,** 510–532.

Dickson, R. R., and J. Brown, 1994: The production of North Atlantic Deep Water: Sources, rates and pathways. *J. Geophys. Res.,* **99** (C6), 12 319–12 341.

——, J. R. N. Lazier, and J. Meincke, 1996: Long term coordinated changes in the convection activity of the North Atlantic. *Prog. Oceanogr.,* **38,** 241–295.

Drange, H., and K. Simonsen, 1996: Formulation of air-sea fluxes in the ESOP2 version of MICOM. Nansen Environmental and Remote Sensing Center, Bergen, Norway, 23 pp.

——, R. Gerdes, Y. Gao, M. Karcher, F. Kauker, and M. Bentsen, 2005: Ocean general circulation modelling of the Nordic Seas. *The Nordic Seas: An Integrated Perspective, Geophys. Monogr.,* Vol. 158, Amer. Geophys. Union, 199–219.

Eden, C., and J. Willebrand, 2001: Mechanism of interannual to decadal variability of the North Atlantic Circulation. *J. Climate,* **14,** 2266–2280.

Eldevik, T., 2002: On frontal dynamics in two model oceans. *J. Phys. Oceanogr.,* **32,** 2915–2925.

Falina, A., A. Sarafanov, and A. Sokov, 2007: Variability and renewal of Labrador Sea Water in the Irminger Basin in 1991–2004. *J. Geophys. Res.,* **112,** C01006, doi:10.1029/2005JC003348.

Flatau, M. K., L. D. Talley, and P. P. Niiler, 2003: The North Atlantic Oscillation, surface current velocities, and SST changes in the subpolar North Atlantic. *J. Climate,* **16,** 2355–2369.

Friedrich, H., and S. Levitus, 1972: An approximation to the equation of state for sea water, suitable for numerical ocean models. *J. Phys. Oceanogr.,* **2,** 514–517.

Ganachaud, A., and C. Wunsch, 2000: Improved estimates of global ocean circulation, heat transport and mixing from hydrographic data. *Nature,* **408,** 453–457.

Gulev, S. K., B. Barnier, H. Knochel, J.-M. Molines, and M. Cottet, 2003: Water mass transformation in the North Atlantic and its impact on the meridional circulation: Insights from an ocean model forced by NCEP–NCAR reanalysis surface fluxes. *J. Climate,* **16,** 3085–3110.

——, T. Jung, and E. Ruprecht, 2007: Estimation of the impact of sampling errors in the VOS observations on air–sea fluxes. Part II: Impact on trends and interannual variability. *J. Climate,* **20,** 302–315.

Haak, H., J. Jungclaus, U. Mikolajewicz, and M. Latif, 2003: Formation and propagation of great salinity anomalies. *Geophys. Res. Lett.,* **30,** 1473, doi:10.1029/2003GL017065.

Häkkinen, S., 1999: Variability of the simulated meridional heat transport in the North Atlantic for the period 1951–1993. *J. Geophys. Res.,* **104** (C5), 10 991–11 008.

——, and P. B. Rhines, 2004: Decline of subpolar North Atlantic Circulation during the 1990s. *Science,* **304,** 555–559.

Hallberg, R., and P. B. Rhines, 1996: Buoyancy-driven circulation in an ocean basin with isopycnals intersecting the sloping boundary. *J. Phys. Oceanogr.,* **26,** 913–940.

Harder, M., 1996: Dynamik, rauhigkeit und alter des meereises in der Arktis. Ph.D. thesis, Alfred-Wegener-Institut fr Polar- und Meeresforschung, Bremerhaven, Germany, 124 pp.

Hátún, H., A. B. Sandø, H. Drange, and M. Bentsen, 2005: Seasonal to decadal temperature variations in the Faroe-Shetland inflow waters. *The Nordic Seas: An Integrated Perspective,* Vol. 158, *Geophys Monogr.,* Amer. Geophys. Union, 239–250.

Josey, S. A., and R. Marsh, 2005: Surface freshwater flux variability and recent freshening of the North Atlantic in the eastern subpolar gyre. *J. Geophys. Res.,* **110,** C05008, doi:10.1029/2004JC002521.

Kalnay, E., and Coauthors, 1996: The NCEP/NCAR 40-Year Reanalysis Project. *Bull. Amer. Meteor. Soc.,* **77,** 437–471.

Kvaleberg, E., and T. W. N. Haine, 2006: Labrador Sea Water transport rates and pathways in the subpolar North Atlantic Ocean. *ASOF Newsl.,* No. 5, 25–27.

Lavender, K. L., R. E. Davis, and W. B. Owens, 2000: Mid-depth recirculation observed in the interior Labrador and Irminger Seas by direct velocity measurements. *Nature,* **407,** 66–69.

Lazier, J. R. N., and D. G. Wright, 1993: Annual velocity variations in the Labrador Current. *J. Phys. Oceanogr.,* **23,** 659–678.

Levitus, S., and T. P. Boyer, 1994: *Temperature*. Vol. 4, *World Ocean Atlas 1994,* NOAA Atlas NESDIS 4, 117 pp.

——, R. Burgett, and T. P. Boyer, 1994: *Salinity.* Vol. 3, *World Ocean Atlas 1994,* NOAA Atlas NESDIS 3, 99 pp.

Marshall, J., and Coauthors, 2001a: North Atlantic climate variability: Phenomena, impacts and mechanisms. *Int. J. Climatol.,* **21,** 1863–1898.

——, H. Johnson, and J. Goodman, 2001b: A study of the inter-

action of the North Atlantic Oscillation with ocean circulation. *J. Climate,* **14,** 1399–1421.

Pickart, R. S., and M. A. Spall, 2007: Impact of Labrador Sea convection on the North Atlantic meridional overturning circulation. *J. Phys. Oceanogr.,* **37,** 2207–2227.

Reverdin, G., P. P. Niiler, and H. Valdimarsson, 2003: North Atlantic Ocean surface currents. *J. Geophys. Res.,* **108,** 3002, doi:10.1029/2001JC001020.

Reynaud, T. H., A. J. Weaver, and R. J. Greatbatch, 1995: Summer mean circulation of the northwestern Atlantic Ocean. *J. Geophys. Res.,* **100** (C1), 779–816.

Schmitt, R. W., P. S. Bogden, and C. E. Dorman, 1989: Evaporation minus precipitation and density fluxes for the North Atlantic. *J. Phys. Oceanogr.,* **19,** 1208–1221.

Schweckendiek, U., and J. Willebrand, 2005: Mechanisms affecting the overturning response in global warming simulations. *J. Climate,* **18,** 4925–4936.

Spall, M. A., 2004: Boundary currents and water mass transformation in marginal seas. *J. Phys. Oceanogr.,* **34,** 1197–1213.

——, and R. S. Pickart, 2003: Wind-driven recirculations and exchange in the Labrador and Irminger Seas. *J. Phys. Oceanogr.,* **33,** 1829–1845.

Straneo, F., 2006: On the connection between dense water formation, overturning and poleward heat transport in a convective basin. *J. Phys. Oceanogr.,* **36,** 1822–1840.

——, R. S. Pickart, and K. L. Lavender, 2003: Spreading of Labrador Sea Water: An advective-diffusive study based on Lagrangian data. *Deep-Sea Res. I,* **50,** 701–719.

Talley, L. D., and M. S. McCartney, 1982: Distribution and circulation of Labrador Sea Water. *J. Phys. Oceanogr.,* **12,** 1189–1204.

Treguier, A. M., S. Theetten, E. P. Chassignet, T. Penduff, R. Smith, L. Talley, J. O. Beismann, and C. W. Bning, 2005: The North Atlantic subpolar gyre in four high-resolution models. *J. Phys. Oceanogr.,* **35,** 757–774.

Trenberth, K. E., and J. M. Caron, 2001: Estimates of meridional atmosphere and ocean heat transports. *J. Climate,* **14,** 3433–3443.

Vellinga, M., and R. A. Wood, 2002: Global climatic impacts of a collapse of the Atlantic thermohaline circulation. *Climatic Change,* **54,** 251–267.

Willebrand, J., and Coauthors, 2001: Circulation characteristics in three eddy-permitting models of the North Atlantic. *Prog. Oceanogr.,* **48,** 123–161.

Yashayaev, I., 2007: Hydrographic changes in the Labrador Sea, 1960–2005. *Prog. Oceanogr.,* **73,** 242–276.